Vectorial Control of Multi-phase Synchronous Motors using POG Approach

Roberto Zanasi
Information Engineering Department
University of Modena e Reggio Emilia
Via Vignolese 905
41100 Modena, Italy
roberto.zanasi@unimore.it

Federica Grossi
Information Engineering Department
University of Modena e Reggio Emilia
Via Vignolese 905
41100 Modena, Italy
federica.grossi@unimore.it

***Abstract*—This paper deals with the vectorial control of multi-phase permanent magnet synchronous machines. The dynamic model of the motor is obtained using the Power-Oriented Graphs technique which clearly shows the power flows within the system and allows to write the dynamic equations of the system in a proper rotating reference frame. Moreover the obtained model can be directly implemented in Simulink. Starting from the model of the motor, a torque control law with saturated input voltages is proposed based on a new "current" approach. The obtained control is very effective and with a simple structure. Simulation results are provided.**

I. Introduction

The dynamic model of multi-phase synchronous motors known in the literature is obtained using classical mathematical methods [1],[2]. In this paper the dynamic model of this type of motors is obtained using a Lagrangian approach in the frame of the Power-Oriented Graphs (POG) technique, see [3],[4],[5]. This graphical modeling technique shows the power flows within the system, allows to write the state space equations of the system in a very compact form and provides a model which can be directly implemented in Simulink. Applying a proper state space transformation the system dynamics is expressed in a rotating frame assuming a very simple form (other approaches have been proposed in [7],[8]).On the basis of the obtained compact model, a vectorial torque control with saturated input voltages is proposed using a new "current" approach. The proposed control law is simple and seems to be more clear than the classical vectorial control which uses a "voltage" approach. The paper is organized as follows. Sec. II introduces the main features of POG technique, Sec. III shows the details of POG dynamic model of the multi-phase synchronous motors and in Sec. IV the new vectorial torque control is presented. In Sec. V some simulation results are finally reported.

II. Power-Oriented Graphs basic principles

The Power-Oriented Graphs technique, see [6], is an energy-based technique suitable for modeling physical systems. The POG are block diagrams combined with a particular modular structure essentially based on the use of the two blocks shown in Fig. 1.a and Fig. 1.b: the *elaboration block* (e.b.) stores and/or dissipates energy (i.e. springs, masses, dampers, capacities, inductances, resistances, etc.); the *connection block* (c.b.) redistributes the power within the system without storing nor dissipating energy (i.e. any type of gear reduction, transformers, etc.). The c.b. transforms the power variables with the constraint $\mathbf{x}_1^{\mathrm{T}}\mathbf{y}_1 = \mathbf{x}_2^{\mathrm{T}}\mathbf{y}_2$. The e.b. and the c.b. are suitable for representing both scalar and vectorial systems. In the vectorial case, $\mathbf{G}(s)$ and $\mathbf{K}$ are matrices: $\mathbf{G}(s)$ is always square, $\mathbf{K}$ can also be rectangular. The circle present in the e.b. is a summation element and the black spot represents a minus sign that multiplies the entering variable. The main feature of the Power-Oriented Graphs is to keep a direct correspondence between the dashed sections of the graphs and real power sections of the modeled systems: the scalar product $\mathbf{x}^{\mathrm{T}}\mathbf{y}$ of the two *power vectors* $\mathbf{x}$ and $\mathbf{y}$ involved in each dashed line of a power-oriented graph, see Fig. 1, has the physical meaning of *the power flowing through that particular section*. The main energetic domains encountered in modeling physical systems are the electrical, the mechanical (translational and rotational) and the hydraulic, see Fig. 1.c. Each energetic domain is characterized by two *power variables*: an *across-variable* v_e defined between two points (i.e. the voltage V), and a *through-variable* v_f defined in each point of the space (i.e. the current I). Another important aspect of the POG technique is the direct correspondence between the POG representations and the corresponding state space descriptions. For example, the POG scheme shown in Fig. 2 can be represented by the state space equations given in (1) where the *energy matrix* $\mathbf{L}$ is symmetric and positive definite: $\mathbf{L} = \mathbf{L}^{\mathrm{T}} > 0$. For such a system, the stored energy E_s and the dissipating power P_d

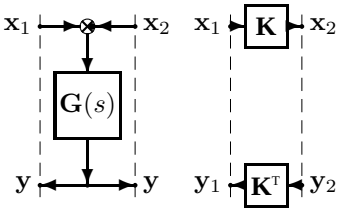

a) *e. b.* b) *c. b.*

	POG Variables	
Domains:	*Across:* v_e	*Through:* v_f
Electrical	Voltage V	Current I
Mec. Tra.	Velocity v	Force F
Mec. Rot.	Ang. Vel. ω	Torque τ
Hydraulic	Pressure P	Flow rate Q

c) *Across and through variables*

Figure 1. POG basic blocks and variables: a) *elaboration block*; b) *connection block*; c) *across and through variables*.

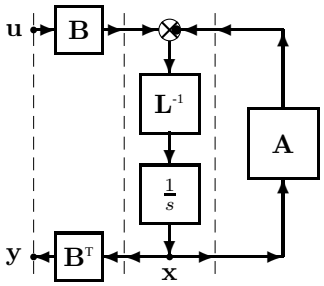

$$\begin{cases} \mathbf{L}\,\dot{\mathbf{x}} = -\mathbf{A}\mathbf{x} + \mathbf{B}\mathbf{u} \\ \mathbf{y} = \mathbf{B}^{\mathrm{T}}\mathbf{x} \end{cases} \quad (1)$$

$$\Downarrow (\mathbf{x} = \mathbf{T}\mathbf{z})$$

$$\begin{cases} \overline{\mathbf{L}}\dot{\mathbf{z}} = -\overline{\mathbf{A}}\mathbf{z} + \overline{\mathbf{B}}\mathbf{u} \\ \mathbf{y} = \overline{\mathbf{B}}^{\mathrm{T}}\mathbf{z} \end{cases} \quad (2)$$

Figure 2. POG block scheme of a generic dynamic system.

can be expressed as follows: $E_s = \frac{1}{2}\mathbf{x}^{\mathrm{T}}\mathbf{L}\,\mathbf{x}$, $P_d = \mathbf{x}^{\mathrm{T}}\mathbf{A}\,\mathbf{x}$. The dynamic model (1) can be transformed and reduced into system (2) using a "congruent" transformation $\mathbf{x} = \mathbf{T}\mathbf{z}$ (matrix $\mathbf{T}$ can be rectangular and time-varying) where $\overline{\mathbf{L}} = \mathbf{T}^{\mathrm{T}}\mathbf{L}\mathbf{T}$, $\overline{\mathbf{A}} = \mathbf{T}^{\mathrm{T}}\mathbf{A}\mathbf{T} - \mathbf{T}^{\mathrm{T}}\mathbf{L}\dot{\mathbf{T}}\mathbf{z}$ and $\overline{\mathbf{B}} = \mathbf{T}^{\mathrm{T}}\mathbf{B}$.

A. Notations

Row matrices will be denoted as follows:

$$\overset{i}{[\![}\, R_i \,\overset{i}{]\!]}_{1:n} = \begin{bmatrix} R_1 & R_2 & \dots & R_n \end{bmatrix},$$

column and diagonal matrices as:

$$\overset{i}{[\![}\, R_i \,]\!]_{1:n} = \begin{bmatrix} R_1 \\ R_2 \\ \vdots \\ R_n \end{bmatrix}, \qquad \overset{i}{[\![}\, R_i \,\overset{i}{]\!]}_{1:n} = \begin{bmatrix} R_1 & & & \\ & R_2 & & \\ & & \ddots & \\ & & & R_n \end{bmatrix}$$

and full matrices as:

$$\overset{i}{[\![}\, R_{i,j} \,\overset{j}{]\!]}_{1:n\ 1:m} = \begin{bmatrix} R_{11} & R_{12} & \cdots & R_{1m} \\ R_{21} & R_{22} & \cdots & R_{2m} \\ \vdots & \vdots & \ddots & \vdots \\ R_{n1} & R_{n2} & \cdots & R_{nm} \end{bmatrix}$$

The symbol "$\sum_{n=a:d}^{b} c_n = c_a + c_{a+d} + c_{a+2d} + \dots$" will be used to represent the sum of a succession of numbers c_n where the index n ranges from a to b with increment d, that is, using the Matlab symbology, $n = [a : d : b]$.
The symbol $\delta(n)|_k^m$ will be used to represent the following function:

$$\delta(n)|_k^m = \begin{cases} 1 & \text{for } n \in [k,\, k \pm m,\, k \pm 2m,\, k \pm 3m, \dots] \\ 0 & \text{otherwise} \end{cases}$$

where n, k and m are integer parameters.

III. Electrical motors modelling

The basic structure of a multi-phase synchronous motor is shown in Fig. 3. In this paper we will refer to a permanent magnet synchronous motor with an *odd* number m_s of star-connected phases [3]-[4] characterized by the parameters shown in Tab. I. Let us introduce the following vectors:

$${}^t\mathbf{I}_s = \begin{bmatrix} I_{s1} \\ I_{s2} \\ \vdots \\ I_{sm_s} \end{bmatrix}, \; {}^t\mathbf{V}_s = \begin{bmatrix} V_{s1} \\ V_{s2} \\ \vdots \\ V_{sm_s} \end{bmatrix}, \; {}^t\dot{\mathbf{q}} = \begin{bmatrix} {}^t\mathbf{I}_s \\ \omega_m \end{bmatrix}, \; {}^t\mathbf{V} = \begin{bmatrix} {}^t\mathbf{V}_s \\ -\tau_e \end{bmatrix} \quad (3)$$

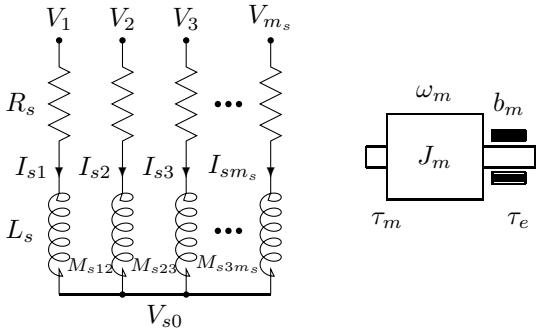

Figure 3. Basic structure of a multi-phase synchronous motor.

m_s	number of motor phases;
p	number of polar expansions;
θ, θ_m	electric and rotor angular positions: $\theta = p\,\theta_m$;
ω, ω_m	electric and rotor angular velocities: $\omega = p\,\omega_m$;
R_s	i-th stator phase resistance;
L_s	i-th stator phase self induction coefficient;
M_{s0}	maximum value of mutual inductance between stator phases;
$\phi_c(\theta)$	total rotor flux chained with stator phase 1;
φ_c	maximum value of function $\phi_c(\theta)$;
J_m	rotor moment of inertia;
b_m	rotor linear friction coefficient;
τ_m	electromotive torque acting on the rotor;
τ_e	external load torque acting on the rotor;
γ_s	basic angular displacement ($\gamma_s = 2\pi/m_s$)

Table I
Parameters of the multi-phase synchronous motor.

where ${}^t\mathbf{I}_s$, ${}^t\mathbf{V}_s$ are the current and voltage stator vectors and ${}^t\dot{\mathbf{q}}$, ${}^t\mathbf{V}$ are the state and input vectors of the global system. Using a "Lagrangian" approach, see [5], one can obtain the following dynamic equations of the electric motor:

$$\underbrace{\left[\begin{array}{c|c} {}^t\mathbf{L}_s & 0 \\ \hline 0 & J_m \end{array}\right]}_{{}^t\mathbf{L}} \underbrace{\begin{bmatrix} {}^t\dot{\mathbf{I}}_s \\ \dot{\omega}_m \end{bmatrix}}_{{}^t\ddot{\mathbf{q}}} = -\underbrace{\left[\begin{array}{c|c} {}^t\mathbf{R}_s & {}^t\mathbf{K}_\tau(\theta) \\ \hline -{}^t\mathbf{K}_\tau^{\mathrm{T}}(\theta) & b_m \end{array}\right]}_{{}^t\mathbf{R} + {}^t\mathbf{W}} \underbrace{\begin{bmatrix} {}^t\mathbf{I}_s \\ \omega_m \end{bmatrix}}_{{}^t\dot{\mathbf{q}}} + \underbrace{\begin{bmatrix} {}^t\mathbf{V}_s \\ -\tau_e \end{bmatrix}}_{{}^t\mathbf{V}} \quad (4)$$

where the energy matrix ${}^t\mathbf{L}_s$ is defined as follows:

$${}^t\mathbf{L}_s = L_{s0}\,\mathbf{I}_{m_s} + M_{s0}\,\overset{i}{[\![}\, \cos((i-j)\gamma_s) \,\overset{j}{]\!]}_{1:m_s\ 1:m_s}$$

with $L_{s0} = L_s - M_{s0}$. Matrices ${}^t\mathbf{R}$ and ${}^t\mathbf{W}$ are defined as:

$${}^t\mathbf{R} = \left[\begin{array}{c|c} {}^t\mathbf{R}_s & 0 \\ \hline 0 & b_m \end{array}\right], \qquad {}^t\mathbf{W} = \left[\begin{array}{c|c} 0 & {}^t\mathbf{K}_\tau(\theta) \\ \hline -{}^t\mathbf{K}_\tau^{\mathrm{T}}(\theta) & 0 \end{array}\right]$$

where ${}^t\mathbf{R}_s = R_s\,\mathbf{I}_{m_s}$ and the torque vector ${}^t\mathbf{K}_\tau(\theta)$ is:

$${}^t\mathbf{K}_\tau(\theta) = p\,\varphi_c \overset{h}{\left\|\left[-\sum_{n=1:2}^{\infty} n\,a_n \sin[n(\theta - h\,\gamma_s)] \right]\right\|}_{0:m_s-1}. \quad (5)$$

The parameters a_n in (5) are the coefficients of the periodic normalized rotor flux function $\bar{\phi}(\theta)$ expressed in Fourier

series: $\bar{\phi}(\theta) = \sum_{n=1:2}^{\infty} a_n \cos(n\theta)$. Let us now consider the following transformation matrix:

$$ {}^{\omega}\mathbf{T}_t = \sqrt{\frac{2}{m_s}} \Bigg\|_{1:2:m_s-2}^{k} \begin{bmatrix} \cos(k\,(\theta - h\,\gamma_s)) \\ \sin(k\,(\theta - h\,\gamma_s)) \end{bmatrix} \Bigg\|_{0:m_s-1}^{h}. \tag{6} $$

Matrix ${}^{\omega}\mathbf{T}_t(\theta)$ is a function of the electrical angle θ and transforms the system variables from the original reference frame Σ_t to a transformed rotating frame Σ_ω. Applying transformation ${}^{t}\dot{\mathbf{q}} = {}^{\omega}\mathbf{T}_t^{\mathrm{T}}\,{}^{\omega}\dot{\mathbf{q}}$ to system (4), one obtains the following transformed system:

$$ \underbrace{\left[\begin{array}{c|c} {}^{\omega}\mathbf{L}_s & 0 \\ \hline 0 & J_m \end{array}\right]}_{{}^{\omega}\mathbf{L}} \underbrace{\left[\begin{array}{c} {}^{\omega}\dot{\mathbf{I}}_s \\ \hline \dot{\omega}_m \end{array}\right]}_{{}^{\omega}\dot{\mathbf{q}}} = - \underbrace{\left[\begin{array}{c|c} {}^{\omega}\mathbf{R}_s + {}^{\omega}\mathbf{L}_s\,{}^{\omega}\mathbf{J}_s & {}^{\omega}\mathbf{K}_\tau(\theta) \\ \hline -\,{}^{\omega}\mathbf{K}_\tau^{\mathrm{T}}(\theta) & b_m \end{array}\right]}_{{}^{\omega}\mathbf{R} + {}^{\omega}\mathbf{W}} \underbrace{\left[\begin{array}{c} {}^{\omega}\mathbf{I}_s \\ \hline \omega_m \end{array}\right]}_{{}^{\omega}\dot{\mathbf{q}}} + \underbrace{\left[\begin{array}{c} {}^{\omega}\mathbf{V}_s \\ \hline -\tau_e \end{array}\right]}_{{}^{\omega}\mathbf{V}} \tag{7} $$

where ${}^{\omega}\mathbf{I}_s = {}^{t}\mathbf{T}_\omega^{\mathrm{T}}\,{}^{t}\mathbf{I}_s$, ${}^{\omega}\mathbf{L}_s = {}^{t}\mathbf{T}_\omega^{\mathrm{T}}\,{}^{t}\mathbf{L}_s\,{}^{t}\mathbf{T}_\omega$, ${}^{\omega}\mathbf{R}_s = {}^{t}\mathbf{T}_\omega^{\mathrm{T}}\,{}^{t}\mathbf{R}_s\,{}^{t}\mathbf{T}_\omega$, ${}^{\omega}\mathbf{J}_s = {}^{t}\mathbf{T}_\omega^{\mathrm{T}}\,{}^{t}\dot{\mathbf{T}}_\omega$, ${}^{\omega}\mathbf{K}_\tau = {}^{t}\mathbf{T}_\omega^{\mathrm{T}}\,{}^{t}\mathbf{K}_\tau$ e ${}^{\omega}\mathbf{V}_s = {}^{t}\mathbf{T}_\omega^{\mathrm{T}}\,{}^{t}\mathbf{V}_s$. Matrices ${}^{\omega}\mathbf{L}_s$ and ${}^{\omega}\mathbf{J}_s$ have the following structure:

$$ {}^{\omega}\mathbf{L}_s = \begin{bmatrix} L_{se} & 0 & 0 & \cdots & 0 \\ 0 & L_{se} & 0 & \cdots & 0 \\ 0 & 0 & L_{s0} & \cdots & 0 \\ \vdots & \vdots & \vdots & \ddots & \vdots \\ 0 & 0 & 0 & \cdots & L_{s0} \end{bmatrix}, \quad {}^{\omega}\mathbf{J}_s = \Bigg\|_{1:2:m_s-2}^{k} \begin{bmatrix} 0 & -k\,\omega \\ k\,\omega & 0 \end{bmatrix}, $$

where $L_{se} = L_{s0} + \frac{m_s}{2} M_{s0}$ and $\omega = \dot{\theta}$ is the time-derivative of the electric angle θ. Vectors ${}^{\omega}\mathbf{I}_s$ and ${}^{\omega}\mathbf{V}_s$ in (7) are now the following:

$$ {}^{\omega}\mathbf{I}_s = \Bigg\|_{1:2:m_s-2}^{k} \begin{bmatrix} {}^{\omega}\mathbf{I}_{sk} \end{bmatrix} \Bigg\| = \Bigg\|_{1:2:m_s-2}^{k} \begin{bmatrix} I_{dk} \\ I_{qk} \end{bmatrix} \Bigg\|, \qquad {}^{\omega}\mathbf{V}_s = \Bigg\|_{1:2:m_s-2}^{k} \begin{bmatrix} {}^{\omega}\mathbf{V}_{sk} \end{bmatrix} \Bigg\| = \Bigg\|_{1:2:m_s-2}^{k} \begin{bmatrix} V_{dk} \\ V_{qk} \end{bmatrix} \Bigg\| $$

where I_{dk}, I_{qk}, V_{dk} and V_{qk} are, respectively, the *direct* and *quadrature* components of the current and voltage vectors ${}^{\omega}\mathbf{I}_s$ and ${}^{\omega}\mathbf{V}_s$. Note that using transformation ${}^{t}\dot{\mathbf{q}} = {}^{\omega}\mathbf{T}_t^{\mathrm{T}}\,{}^{\omega}\dot{\mathbf{q}}$, the original state space Σ_t has been transformed into $(m_s - 1)/2$ two-dimensional orthogonal subspaces named $\Sigma_{\omega k}$ with $k \in \{1 : 2 : m_s - 2\}$. A detailed discussion of the properties of the components of vector ${}^{\omega}\mathbf{K}_\tau(\theta)$ can be found in [4]. It can be shown, see [5], that when the rotor flux function $\bar{\phi}(\theta)$ has the following structure:

$$ \bar{\phi}(\theta) = \sum_{i=1:2}^{m_s-2} a_i \cos(i\,\theta) \tag{8} $$

the torque vector ${}^{\omega}\mathbf{K}_\tau(\theta)$ is constant (i.e. it is not function of the electric angle θ) with the following expression:

$$ {}^{\omega}\mathbf{K}_\tau = -\varphi_c\,p\,\sqrt{\frac{m_s}{2}} \Bigg\|_{1:2:m_s-2}^{k} \begin{bmatrix} 0 \\ k\,a_k \end{bmatrix} \Bigg\| = \Bigg\|_{1:2:m_s-2}^{k} \begin{bmatrix} {}^{\omega}\mathbf{K}_{\tau k} \end{bmatrix} \Bigg\| = \Bigg\|_{1:2:m_s-2}^{k} \begin{bmatrix} K_{dk} \\ K_{qk} \end{bmatrix} \Bigg\| \tag{9} $$

The POG scheme of the synchronous motor in the transformed space Σ_ω, see eq. (7), is shown in Fig. 4. The elaboration blocks present between the power sections ② and ③ represent

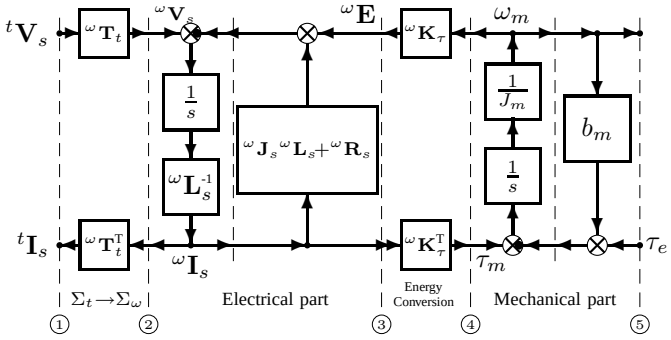

Figure 4. POG scheme of a multi-phase electrical motor in the transformed space Σ_ω.

the *Electrical part* of the system, while the blocks present between sections ④ and ⑤ represent the *Mechanical part* of the system. The connection blocks present between sections ① and ② and between sections ③ and ④ represent, respectively, the state space transformation ${}^{t}\mathbf{T}_\omega$ between reference frames Σ_t and Σ_ω, and the energy and power conversion (without accumulation nor dissipation) between the electrical and mechanical parts of the motor.

A. Balanced voltages

Let us now consider the case of balanced input voltages ${}^{t}\mathbf{V}_s$ with the following structure:

$$ {}^{t}\mathbf{V}_s = \Big\|_{1:m_s}^{h} [\![\, V_{sh} \,]\!] = \Big\|_{1:m_s}^{h} [\![\, V_m\, \cos(k_1((h-1)\gamma_s - \theta_1)) \,]\!] \tag{10} $$

where V_m is the maximum value of the input voltage and k_1, θ_1 denote the following parameters:

$$ k_1 \in \{1 : 2 : m_s - 2\}, \qquad \theta_1 = \theta + \theta_s $$

where θ_s is a proper initial phase shift. The transformed vector ${}^{\omega}\mathbf{V}_s = {}^{t}\mathbf{T}_\omega^{\mathrm{T}}\,{}^{t}\mathbf{V}_s$ has the following structure:

$$ {}^{\omega}\mathbf{V}_s = \sqrt{\frac{2}{m_s}} \Bigg\|_{1:2:m_s-2}^{k} \begin{bmatrix} \displaystyle\sum_{h=0}^{m_s-1} V_m \cos(k_1 h\,\gamma_s - k_1\theta_1)\cos(k\,h\,\gamma_s - k\,\theta) \\ \displaystyle\sum_{h=0}^{m_s-1} V_m \cos(k_1 h\,\gamma_s - k_1\theta_1)\sin(k\,h\,\gamma_s - k\,\theta) \end{bmatrix} \Bigg\|. $$

Using simple mathematical elaborations it can be shown that the vector ${}^{\omega}\mathbf{V}_s$ gets the following simplified structure:

$$ {}^{\omega}\mathbf{V}_s = \sqrt{\frac{m_s}{2}}\, V_m \Bigg\|_{1:2:m_s-2}^{k} \begin{bmatrix} \delta(k_1 - k)|_0^{m_s} \cos(k\,\theta_s) \\ \delta(k_1 - k)|_0^{m_s} \sin(k\,\theta_s) \end{bmatrix} \Bigg\|. \tag{11} $$

Note that in vector ${}^{\omega}\mathbf{V}_s$ the only components that are different from zero are the two components for which $k = k_1$. Using the

following bijective correspondence between two-dimensional vectors and complex numbers:

$$\begin{bmatrix}\cos(k\,\theta_s)\\ \sin(k\,\theta_s)\end{bmatrix} \quad \leftrightarrow \quad \cos(k\,\theta_s)+j\,\sin(k\,\theta_s)=e^{j\,k\,\theta_s}$$

the expression (11) can be rewritten as follows:

$${}^{\omega}\mathbf{V}_s=\sqrt{\frac{m_s}{2}}\,V_m\left\|\left[\begin{array}{c}k\\ \delta(k_1-k)|_0^{m_s}\;e^{j\,k\,\theta_s}\end{array}\right]\right\|_{1:2:m_s-2}. \qquad (12)$$

Expression (12) shows that all the balanced input vectors ${}^{t}\mathbf{V}_s$ with bounded amplitude V_m, see (10), are transformed into vectors ${}^{\omega}\mathbf{V}_s$ which belong to a circle with radius $V_{\overline{M}}=\sqrt{\frac{m_s}{2}}\,V_m$ in the two-dimensional subspace $\Sigma_{\omega k_1}$.

IV. Vectorial Control

Let ${}^{\omega}\mathbf{I}_d$ denote the constant desired current. The condition ${}^{\omega}\mathbf{I}_s={}^{\omega}\mathbf{I}_d$ can be achieved using the following control law:

$${}^{\omega}\mathbf{V}_s=({}^{\omega}\mathbf{R}_s+{}^{\omega}\mathbf{L}_s\,{}^{\omega}\mathbf{J}_s)\,{}^{\omega}\mathbf{I}_s+{}^{\omega}\mathbf{K}_\tau\,\omega_m-\mathbf{K}_c({}^{\omega}\mathbf{I}_s-{}^{\omega}\mathbf{I}_d) \quad (13)$$

where $\mathbf{K}_c>0$ is a diagonal matrix used for the tuning of the control. Putting relation (13) in (7) one obtains the two following decoupled dynamic equations:

$$\left\{\begin{array}{rcl}{}^{\omega}\mathbf{L}_s\,{}^{\omega}\dot{\mathbf{I}}_s &=& -\mathbf{K}_c({}^{\omega}\mathbf{I}_s-{}^{\omega}\mathbf{I}_d)\\ J_m\,\dot{\omega}_m &=& {}^{\omega}\mathbf{K}_\tau^{\mathrm{T}}\,{}^{\omega}\mathbf{I}_s-b_m\,\omega_m-\tau_e\end{array}\right. \qquad (14)$$

Let ${}^{\omega}\tilde{\mathbf{I}}_s=({}^{\omega}\mathbf{I}_s-{}^{\omega}\mathbf{I}_d)$ denote the current error vector. Since ${}^{\omega}\mathbf{L}_s\,{}^{\omega}\dot{\mathbf{I}}_d=0$, the first equation of system (14) can be rewritten as follows:

$${}^{\omega}\mathbf{L}_s\,{}^{\omega}\dot{\tilde{\mathbf{I}}}_s=-\mathbf{K}_c\,{}^{\omega}\tilde{\mathbf{I}}_s\,. \qquad (15)$$

With a proper choice of matrix $\mathbf{K}_c$ it is possible to define arbitrarily the time constant τ_i of the controlled system:

$$\mathbf{K}_c=\left\|\left[\begin{array}{c}i\\ K_{c_i}\end{array}\right]\right\|_{1:m_s}=\left\|\left[\begin{array}{c}i\\ \frac{{}^{\omega}L_{si}}{\tau_i}\end{array}\right]\right\|_{1:m_s}\quad\rightarrow\quad \tau_i=\frac{{}^{\omega}L_{si}}{K_{c_i}} \qquad (16)$$

where ${}^{\omega}L_{si}$ and K_{c_i} are the i-th diagonal elements of matrices ${}^{\omega}\mathbf{L}_s$ and $\mathbf{K}_c$, respectively. From (15) and (16) it is evident that after a transient the error vector ${}^{\omega}\tilde{\mathbf{I}}_s$ tends asymptotically to zero (i.e. ${}^{\omega}\mathbf{I}_s$ tends to ${}^{\omega}\mathbf{I}_d$) with the desired time constants τ_i.

A. Saturated vectorial control

When ${}^{\omega}\mathbf{I}_s={}^{\omega}\mathbf{I}_d$, the control law (13) is equivalent to $(m_s-1)/2$ two-dimensional decoupled control laws:

$${}^{\omega}\mathbf{V}_{sk}=({}^{\omega}\mathbf{R}_{sk}+{}^{\omega}\mathbf{J}_{sk}\,{}^{\omega}\mathbf{L}_{sk})\,{}^{\omega}\mathbf{I}_{sk}+{}^{\omega}\mathbf{K}_{\tau k}\,\omega_m \qquad (17)$$

where:

$${}^{\omega}\mathbf{R}_{sk}=\begin{bmatrix}R_s & 0\\ 0 & R_s\end{bmatrix},\quad {}^{\omega}\mathbf{J}_{sk}\,{}^{\omega}\mathbf{L}_{sk}=\begin{bmatrix}0 & -k\,p\,\omega_m L_{sk}\\ k\,p\,\omega_m L_{sk} & 0\end{bmatrix}$$

for $k\in\{1:2:m_s-2\}$, each one acting on subspace $\Sigma_{\omega k}$ and

$$L_{sk}=\left\{\begin{array}{ll}L_{se} & \text{for } k=1\\ L_{s0} & \text{for } k\in\{3,\,5,\,7,\ldots,m_s\}\end{array}\right.$$

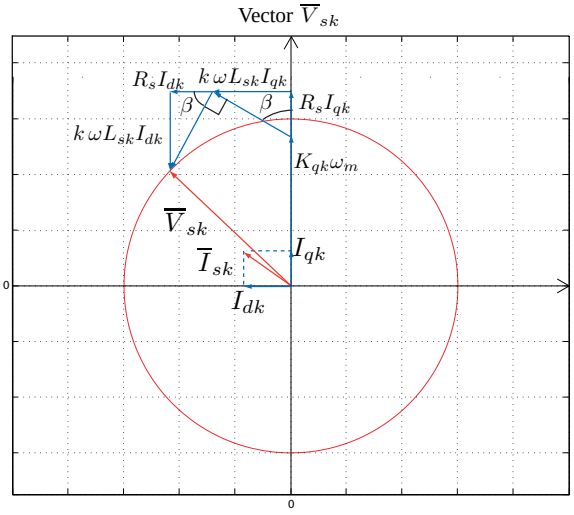

Figure 5. Graphical representation of vector $\overline{V}_{sk}$ on plane $\Sigma_{\omega k}$.

Using the following bijective correspondences between two-dimensional vectors and complex numbers:

$${}^{\omega}\mathbf{I}_{sk}\leftrightarrow\overline{I}_{sk}=I_{dk}+j\,I_{qk},\quad {}^{\omega}\mathbf{V}_{sk}\leftrightarrow\overline{V}_{sk}=V_{dk}+j\,V_{qk},$$

$${}^{\omega}\mathbf{K}_{\tau k}\leftrightarrow\overline{K}_{\tau k}=K_{dk}+j\,K_{qk},\quad {}^{\omega}\mathbf{J}_{sk}\,{}^{\omega}\mathbf{L}_{sk}\leftrightarrow j\,k\,p\,\omega_m L_{sk}$$

and ${}^{\omega}\mathbf{R}_{sk}\leftrightarrow R_s$, eq. (17) can be rewritten as follows:

$$\overline{V}_{sk}=(R_s+j\,k\,p\,\omega_m L_{sk})\overline{I}_{sk}+\overline{K}_{\tau k}\,\omega_m \qquad (18)$$

where j is the imaginary unit number. When vector ${}^{\omega}\mathbf{K}_\tau$ is constant, see (9), then $\overline{K}_{\tau k}=j\,K_{qk}$ and from (18) one obtains the following "voltage" relation:

$$\overline{V}_{sk}=j(R_s I_{qk}+K_{qk}\omega_m)-k\,\omega L_{sk} I_{qk}+(R_s+j\,k\,\omega L_{sk})I_{dk}$$

which is graphically represented in Fig. 5 on the complex plane $\Sigma_{\omega k}$ when vector $\overline{V}_{sk}$ reaches the maximum circle of radius $V_{\overline{M}}$, see [1]. A different "current" approach to the saturated vectorial control can be obtained, when $\overline{K}_{\tau k}=j\,K_{qk}$, rewriting relation (18) as follows:

$$\begin{array}{rcl}\overline{I}_{sk} &=& \dfrac{\overline{V}_{sk}-j\,K_{qk}\,\omega_m}{R_s+j\,k\,p\,\omega_m\,L_{sk}}\\ &=& \underbrace{\dfrac{\overline{V}_{sk}}{R_s+j\,k\,p\,\omega_m\,L_{sk}}}_{\overline{R}_{0k}\,(\omega_m)}+\underbrace{\dfrac{-j\,K_{qk}\,\omega_m}{R_s+j\,k\,p\,\omega_m\,L_{sk}}}_{\overline{C}_{0k}\,(\omega_m)}\end{array}. \qquad (19)$$

When vector $\overline{V}_{sk}$ varies along the bounding circle, relation (19) provides the corresponding limit values for the stator current vector $\overline{I}_{sk}$. Fig. 6 shows a graphical representation of relation (19) when $\overline{V}_{sk}$ varies along the bounding circle for some values of the angular velocity ω_m. The term $\overline{C}_{0k}\,(\omega_m)$ in (19) can be written as:

$$\overline{C}_0(\omega_m)=\underbrace{\frac{-K_{qk}\,k\,p\,\omega_m^2 L_{sk}}{R_s^2+k^2\,p^2\,\omega_m^2 L_{sk}^2}}_{X_{0k}(\omega_m)}+j\,\underbrace{\frac{-K_{qk}\,\omega_m R_s}{R_s^2+k^2\,p^2\,\omega_m^2 L_{sk}^2}}_{Y_{0k}(\omega_m)} \qquad (20)$$

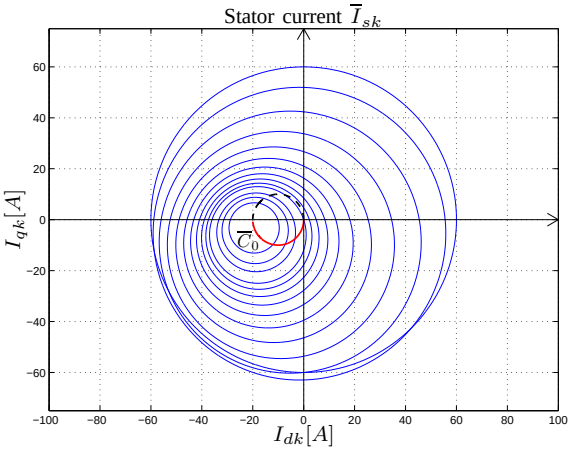

Figure 6. Limit values of stator current $\overline{I}_{sk}$ for some values of ω_m.

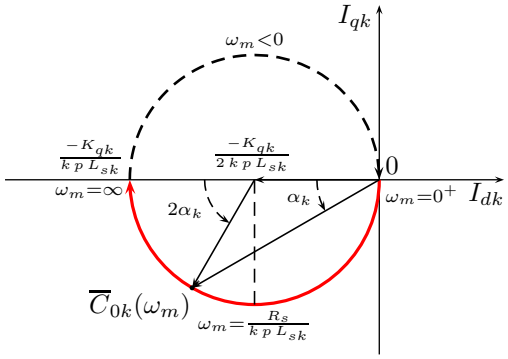

Figure 7. Point $\overline{C}_{0k}(\omega_m)$ moving in the plane $\Sigma_{\omega k}$ varying ω_m.

It can be shown that, varying ω_m, point $\overline{C}_{0k}(\omega_m)$ moves in the complex plane $\Sigma_{\omega k}$ on a circle with center in $\frac{-K_{qk}}{2\,k\,p\,L_{sk}}$, radius $\frac{K_{qk}}{2\,k\,p\,L_{sk}}$, see Fig. 7, and parameter $\alpha_k(\omega_m)$ defined as:

$$\alpha_k(\omega_m) = \arctan \frac{R_s}{k\,p\,\omega_m L_{sk}}. \tag{21}$$

As the voltage $\overline{V}_{sk}$ varies along the bounding circle, the term $\overline{R}_{0k}(\omega_m)$ in (19) has the following expression:

$$\overline{R}_{0k}(\omega_m) = \frac{V_{\overline{M}}\, e^{j\,\varphi}}{R_s + j\,k\,p\,\omega_m\,L_{sk}} = R_{0k}(\omega_m)\, e^{j\,(\,\varphi\,+\,\beta_k)} \tag{22}$$

where $\varphi = [0 : 2\pi]$ and with $R_{0k}(\omega_m)$ and β_k defined as:

$$R_{0k}(\,\omega_m) = \frac{V_{\overline{M}}}{\sqrt{R_s^2 + k^2\,p^2\,\omega_m^2 L_{sk}^2}},\ \beta_k = \arctan \frac{k\,p\,\omega_m L_{sk}}{R_s} \tag{23}$$

Equation (22) puts in evidence that $\overline{R}_{0k}(\omega_m)$ is a circle whose radius $R_{0k}(\omega_m)$ depends on ω_m. The limit value of ω_m over which the circle given in (19) does not intersect axis $I_{dk} = 0$ can be determined by imposing $\overline{R}_{0k}\,(\omega_m) = -X_{0k}\,(\omega_m)$. Fig. 8 shows a geometric representation of the current vector $\overline{I}_{sk}$ for some ω_m and the points I_{qkM}, I_{qkN}, I_{qkn} and I_{qkm} which are important for the control. The red circle shown in Fig. 8 refers to a particular value of ω_m. The projection of all the points of the red circle on the I_{qk} axis gives the range of the currents which can generate torque satisfying the constraint

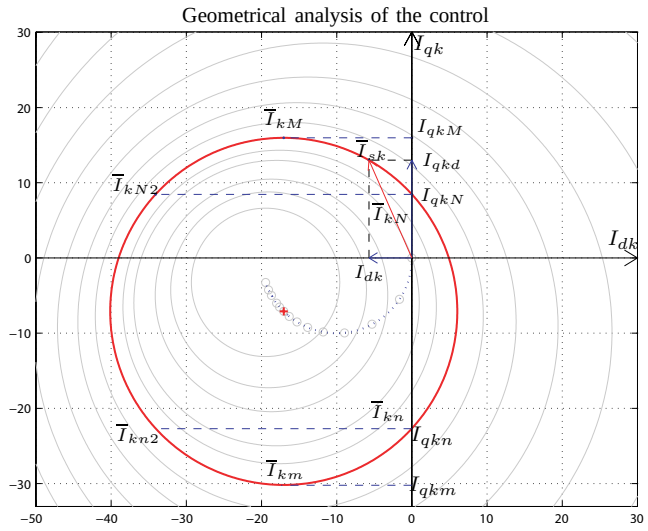

Figure 8. Modulation and translation on current $\overline{I}_{sk}$ for a generic ω_m. The main points useful for the control are shown.

on the maximum input voltage. Three operative zones are defined: 1) the zone between I_{qkn} and I_{qkN} represents the zone in which the torque can be provided using only the quadrature component I_{qk} of the current vector $\overline{I}_{sk}$; 2) the intervals $[I_{qkm},\ I_{qkn}]$ and $[I_{qkN},\ I_{qkM}]$ represent the zone in which the desired torque can be provided giving also a proper direct component I_{dk} to vector $\overline{I}_{sk}$; 3) the zone where $I_{qk} > I_{qkM}$ and $I_{qk} < I_{qkn}$ is not allowed because it does not satisfy the constraint on the maximum input voltage. The coordinates of the main points represented in Fig. 8 are:

$$\begin{aligned}
\overline{I}_{kM}(\omega_m) &= X_{0k}(\omega_m) + j[Y_{0k}(\omega_m) + R_{0k}(\omega_m)] \\
\overline{I}_{km}(\omega_m) &= X_{0k}(\omega_m) + j[Y_{0k}(\omega_m) - R_{0k}(\omega_m)] \\
\overline{I}_{kN}(\omega_m) &= j[\sqrt{R_{0k}^2(\omega_m) - X_{0k}^2(\omega_m)} + Y_{0k}(\omega_m)] \\
\overline{I}_{kn}(\omega_m) &= j[Y_{0k}(\omega_m) - \sqrt{R_{0k}^2(\omega_m) - X_{0k}^2(\omega_m)}]
\end{aligned}$$

The control algorithm which, in each instant, provides the current vector $\overline{I}_{sk}$ closest to the desired current I_{qkd} corresponding to the desired torque τ_d and satisfying the voltage constraint, is the following:

$$\overline{I}_{sk} = \begin{cases} \overline{I}_{kM} & \text{if } I_{qkd} \geq I_{qkM} \\ \overline{I}_{kv} & \text{if } (I_{qkN} < I_{qkd} < I_{qkM}) \wedge (I_{qkm} < I_{qkd} < I_{qkn}) \\ j\,I_{qkd} & \text{if } I_{qkn} < I_{qkd} < I_{qkN} \\ \overline{I}_{km} & \text{if } I_{qkd} \leq I_{qkm} \end{cases}$$

where $\overline{I}_{kv} = X_{0k} + \sqrt{R_{0k}^2 - (I_{qkd} - Y_{0k})^2} + j\,I_{qd}$.

V. Simulation

The controlled electric motor has been implemented in Simulink according to the POG scheme of Fig. 4. The simulation results have been obtained using the following electrical and mechanical parameters: $m_s = 5$, $p = 1$, $R_s = 2\,\Omega$, $L_s = 0.03$ H, $M_{s0} = 0.025$ H, $\varphi_c = 0.6$ W, $J_m = 1.6$ kg m^2, $b_m = 0.8$ Nm s/rad. The external torque τ_e is zero until $t = 15$

s then $\tau_e = 5$ Nm (see the black dashed line in Fig. 9) and the desired torque is $\tau_d = 42$ Nm until $t = 21$ s then $\tau_d = 24$ Nm. The control is executed in the subspace $\Sigma_{\omega 1}$. Fig. 9

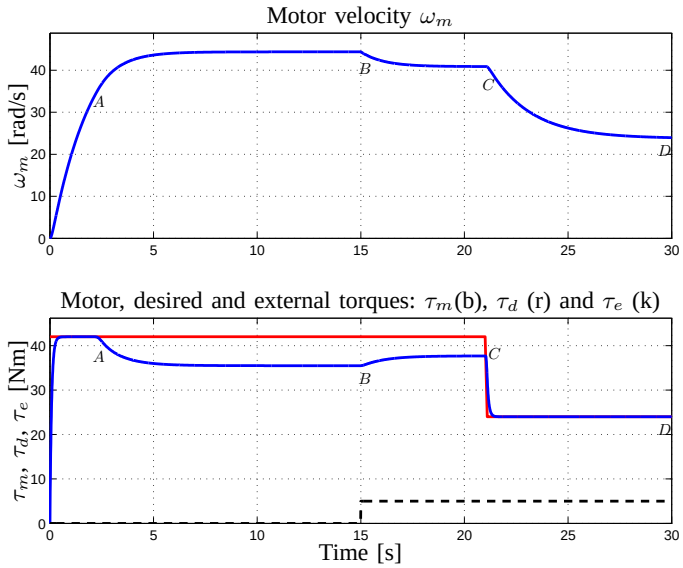

Figure 9. Motor velocity ω_m and motor, desired and external torques: τ_m, τ_d and τ_e torques.

shows the motor velocity ω_m and the torques: motor torque τ_m, desired torque τ_d and applied external torque τ_e. In the figures the letters A, B, C and D remind the critical points: A when the voltage reaches its maximum value, B when the external torque is applied, C when the desired torque switches to $\tau_d = 24$ Nm and D is the final steady state condition. The stator voltages and currents are shown in Fig. 10 from 20 s to 22 s. In Fig. 11 the voltage vector $\overline{V}_{s1}$ is reported: the red dashed line is the bounding circle (see Fig. 5). Fig. 12 shows the motor torque τ_m as function of velocity ω_m, the curve of the maximum torque and the two load torque lines (for $\tau_e = 0$ Nm and $\tau_e = 5$ Nm).

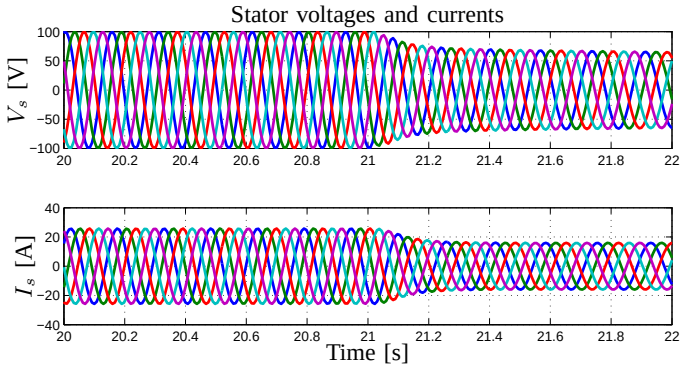

Figure 10. Voltages and current vectors of stator phases.

VI. Conclusion

In this paper the vectorial control of multi-phase synchronous machines with saturated input is analyzed. With

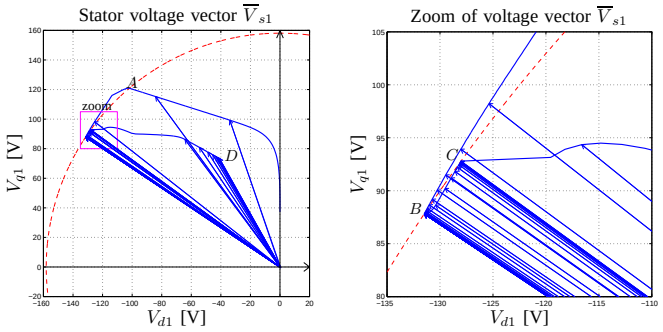

Figure 11. Stator voltage vector $\overline{V}_{s1}$ and zoom.

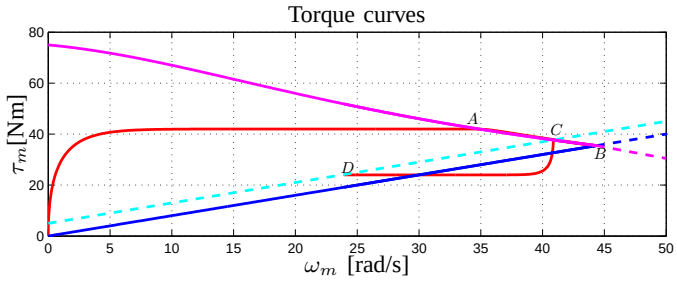

Figure 12. Limit velocity of the motor ω_m in the intersection between the load torque line and the maximum torque curve.

the use of Power-Oriented Graphs technique the dynamic model of the motor is obtained together with the state space equations of the system. The obtained model has been directly implemented in Simulink. Starting from the model of the motor, a vectorial torque control law has been proposed based on a new "current" approach leading to a very simple and effective control. Simulation results are provided and show the effectiveness of the proposed vectorial control in the case of a five-phase motor.

Acknowledgment

The authors gratefully thank Dr. Stefano Puccini for helping in the implementation of control algorithm and simulations.

References

[1] Peter Vas, *Vector Control of AC Machines*, Clarendon press, Oxford, 1990.
[2] W. Leonhard, *Control of Electrical Drives*, 3rd Edition 2001, Springer-Verlag Berlin Heidelberg NewYork, ISBN 3-540-41820-2.
[3] R. Zanasi, F. Grossi "The POG technique for modelling multi-phase permanent magnet synchronous motors", 6th EUROSIM Congress on Modelling and Simulation, Ljubljana, 9-13 September 2007.
[4] R. Zanasi, F. Grossi, "Multi-phase Synchronous Motors: POG Modeling and Optimal Shaping of the Rotor Flux", ELECTRIMACS 2008, Québec, Canada, June 2008.
[5] R. Zanasi, F. Grossi "Optimal Rotor Flux Shape for Multi-phase Permanent Magnet Synchronous Motors", International Power Electronics and Motion Control Conference, September 1-3 2008, Poznan, Poland.
[6] Zanasi R., "Dynamics of a n-links Manipulator by Using Power-Oriented Graph", *SYROCO '94*, Capri, Italy, 1994.
[7] X. Kestelyn, E. Semail, JP. Hautier, "Vectorial Multi-machine Modeling for a Five-Phase Machine", in Proc. Int. Conf. Electrical Machines (ICEM), Bruges, Belgium, 2002, CD-ROM, Paper 394.
[8] E. Semail, X. Kestelyn, A. Bouscayrol, "Right Harmonic Spectrum for the Back-Electromotive Force of a n-phase Synchronous Motor", Industry Applications Conference, 2004, 39th IAS Annual Meeting, ISBN: 0-7803-8486-5.